SI0100124

Nuclear Energy in Central Europe '98
Terme Čatež, September 7 to 10, 1998

ESE a 2D Compressible Multiphase Flow Code Developed for MFCI Analysis – Code Description

Matjaž Leskovar
"Jožef Stefan" Institute
Jamova 39, 1000 Ljubljana, Slovenia
E-mail: matjaz.leskovar@ijs.si, http://www2.ijs.si/~mleskovar/

ABSTRACT - The ESE (Evaluation of Steam Explosions) computer code has been developed to model the interaction of molten core debris with water during the first premixing stage of a steam explosion. A steam explosion is a physical event, which may occur during a severe reactor accident following core meltdown when the molten fuel comes into contact with the coolant water.

In this paper the numerical treatment of probabilistic multiphase flow equations on which ESE is based is described. ESE is a general two-dimensional compressible multiphase flow computer code. Each phase in the multiphase flow – usually water, steam, melt and air – is represented by one flow field with its own local concentration and temperature and is described with its own set of partial differential mass, momentum and energy equations. These transport equations are solved on a staggered grid in a 2D rectangular or cylindrical coordinate system using a high-resolution finite difference method. The pressure equation is solved using the stabilized squared conjugate gradient method (CGSTAB), which converges fast also for high density ratios.

The numerical methods used in ESE were precisely tested on a number of carefully chosen cases where the analytical solutions are known. All results are presented in form of graphs and they clearly show that the applied high-resolution method most exactly reproduces the analytical behavior.

Nomenclature

c_p	specific heat
E	heat transfer
Fr_0	Froude number $v_0/\sqrt{g_0 l_0}$
$\vec{\mathbf{g}}$	gravity
h	enthalpy
Δh	interphase enthalpy difference
l	length
$\vec{\mathbf{M}}$	friction
Ma	Mach number $v_0/(cv_0)=1/c$
p	pressure
Pe_0	Peclet number $v_0 l_0 c_{p0}\rho_0/\lambda_0$
Re_0	Reynolds number $v_0 l_0 \rho_0/\mu_0$
t	time
Δt	time step
$\vec{\mathbf{v}}$	velocity
$\Delta\vec{\mathbf{v}}$	interphase velocity difference
x, r, z	spatial coordinates
V	volume

Greek Letters

α	phase presence probability
β	thermal dilatation
χ	compressibility
λ	thermal conductivity
μ	dynamic viscosity
Γ	vapor generation
ρ	density

Subscripts / Superscripts

0	characteristic value
h	constant enthalpy
i	mesh point
n	time step
p	phase or pressure

1. Introduction

The paper describes the numerical treatment of the probabilistic multiphase flow equations on which the computer code ESE (Evaluation of Steam Explosions) is based. ESE has been developed to model the interaction of molten core debris with water during the first premixing stage of a steam explosion [1]. A steam explosion is a physical event, which may occur during a severe reactor accident following core meltdown when the molten fuel comes into contact with the coolant water.

Many other premixing codes exist in the literature, e.g. CHYMES [2], IFCI [3], PM-ALPHA [4], MC3D [5], IVA3 [6] and COMETA [7]. The common feature of these codes is that they are based on first order accurate numerical methods, whereas ESE uses the second order accurate high-resolution method. High-resolution methods combine first and second order accurate numerical schemes in such a way that the weaknesses of both schemes, the poor numerical accuracy and large amount of numerical dissipation of first order accurate numerical schemes and the oscillations of second order accurate numerical schemes occurring in the vicinity of non-smooth solutions, are suppressed and the method still remains second order accurate [8].

2. Numerical Treatment of Multiphase Flow Equations

Each phase in the multiphase flow is described using the probabilistic mass

$$\frac{\partial}{\partial t}(\alpha\rho)+\nabla\cdot(\alpha\rho\vec{\mathbf{v}})=\Gamma, \tag{1}$$

momentum

$$\rho\frac{\partial\vec{\mathbf{v}}}{\partial t}+\rho(\vec{\mathbf{v}}\cdot\nabla)\vec{\mathbf{v}}=-\frac{1}{\mathrm{Fr}_0^2}\nabla p+\frac{1}{\mathrm{Fr}_0^2}\rho\vec{\mathbf{g}}+\frac{1}{\mathrm{Re}_0}\vec{\mathbf{M}}+\frac{\Delta\vec{\mathbf{v}}\Gamma}{\alpha} \tag{2}$$

and energy equations

$$\rho\frac{\partial h}{\partial t}+\rho(\vec{\mathbf{v}}\cdot\nabla)h=\frac{1}{\mathrm{Pe}_0}E+\frac{\Delta h\Gamma}{\alpha} \tag{3}$$

obtained by ensemble averaging [9]. The mass equation (1) is solved in conservative form to achieve mass conservation, whereas the momentum (2) and energy equations (3) are solved in nonconservative form since the numerical solution of the conservative form of the momentum and energy equations did not give the correct results at non-smooth distributions of the phase presence probability α occurring at phase interfaces.

The discretised multiphase flow equations (1-3) are solved in 2D cartesian or cylindrical coordinate system on a staggered grid using a high-resolution finite difference method. High-resolution methods assure second order accuracy and give well resolved, nonoscillatory discontinuities. The applied high-resolution method is based on the first order time and space accurate upwind scheme and the second order time and space accurate Lax-Wendroff scheme. The total variation diminishing (TVD) condition for the convective terms was satisfied by choosing the smooth van Leer flux-limiter function.

To allow also the treatment of shock waves, the discretisation of the convective term in the nonconservative momentum equation (2) had to be carried out in a special way

$$\left[(\vec{\mathbf{v}}\cdot\nabla)\vec{\mathbf{v}}\right]_i=\max(v_{i-1},v_i,v_{i+1})\left[\frac{\partial v}{\partial x}\right]_i, \tag{4}$$

since otherwise the shock would not propagate if the velocity in front of the shock would be zero. For better clarity the discretisation was presented only for positive velocities and in only one dimension.

The pressure equation for the assumed common pressure field p was derived from the sum of the conservative form of the compressible flow continuity equation (1) over all phases using the projection method

$$1=\sum_p \frac{1}{\rho^{n+1/2}}\left(\alpha^{n+1}\rho^n+\Gamma^{n+1}\Delta t-\nabla\left(\alpha^{n+1}\rho^{n+1/2}\vec{\mathbf{v}}_{\neq p}^{n+1}\right)\Delta t+\left(\Delta t^2\right)\nabla\left(\alpha^{n+1}\rho^{n+1/2}\frac{1}{\mathrm{Fr}_0^2\rho^n}\nabla p^{n+1}\right)\right)+$$
$$+\sum_p \frac{1}{\rho^{n+1/2}}\frac{\left(p^n-p^{n+1}\right)}{\rho^{n+1/2}}\frac{\mathrm{Ma}^2}{\mathrm{Fr}_0^2}\left(\begin{array}{l}\alpha^{n+1}\rho^n+\Gamma^{n+1}\Delta t-\nabla\left(\alpha^{n+1}\rho^{n+1/2}\vec{\mathbf{v}}_{\neq p}^{n+1}\right)\Delta t+\\ +\left(\Delta t^2\right)\nabla\left(\alpha^{n+1}\rho^{n+1/2}\frac{1}{\mathrm{Fr}_0^2\rho^n}\nabla p^n\right)\end{array}\right)+ \qquad (5)$$
$$+\sum_p \frac{1}{\rho^{n+1/2}}\nabla\left(\alpha^{n+1}\frac{\mathrm{Ma}^2}{\mathrm{Fr}_0^2}\left(\vec{\mathbf{v}}_{\neq p}^{n+1}-\frac{\Delta t}{\mathrm{Fr}_0^2\rho^n}\nabla p^n\right)\left(p^n-p^{n+1}\right)\right)\Delta t,$$

where

$$\vec{\mathbf{v}}^{n+1}=\vec{\mathbf{v}}^{n+1/2}+\Delta\vec{\mathbf{v}}_p=\vec{\mathbf{v}}^{n+1/2}-\frac{\Delta t}{\mathrm{Fr}_0^2\rho^n}\left(\nabla p^{n+1}-\nabla p^n\right)=\vec{\mathbf{v}}_{\neq p}^{n+1}-\frac{\Delta t}{\mathrm{Fr}_0^2\rho^n}\nabla p^{n+1} \qquad (6)$$

and

$$\rho^{n+1}=\rho^{n+1/2}+\Delta\rho_p=\rho^{n+1/2}+\left(\frac{\partial\rho}{\partial p}\right)_h\left(p^{n+1}-p^n\right),\rho^{n+1/2}=\rho\left(h^{n+1},p^n\right),\left(\frac{\partial\rho}{\partial p}\right)_h=\frac{\mathrm{Ma}^2}{\mathrm{Fr}_0^2}. \qquad (7)$$

Despite the similarity in appearance to the pressure equation for incompressible flows, there are important differences. The incompressible pressure equation is a Poisson equation, i.e. the coefficients in the discretised form represent an approximation to the Laplacian operator. In the compressible case, there are contributions that represent the fact that the equation for the pressure in a compressible flow contains beside diffusive terms also convective and unsteady terms. At low Mach numbers, the Laplacian term dominates and we recover the Poisson equation. On the other hand, at high Mach numbers, the convective term dominates, reflecting the hyperbolic nature of the flow. Thus this compressible flow pressure equation (5) automatically adjusts to the local nature of the flow and therefore can be applied to all types of flow including also the treatment of temperature expansion.

The pressure equation is solved using the stabilized squared conjugate gradient method (CGSTAB) [10], which was chosen since it converges fast also for high density ratios. The convergence rate of the CGSTAB method was tested for different density ratios of a two phase flow (rise of a big bubble) and was compared with other proposed pressure equation solvers - the Alternate Direction Implicit solver (ADI) and the Stones Strongly Implicit Procedure (SIP). As seen on Fig.1, it was found out that the used CGSTAB method has the fastest convergence rate, which is nearly independent on the density ratio, whereas the ADI and SIP methods become useless if the density ratio is greater than about 1000.

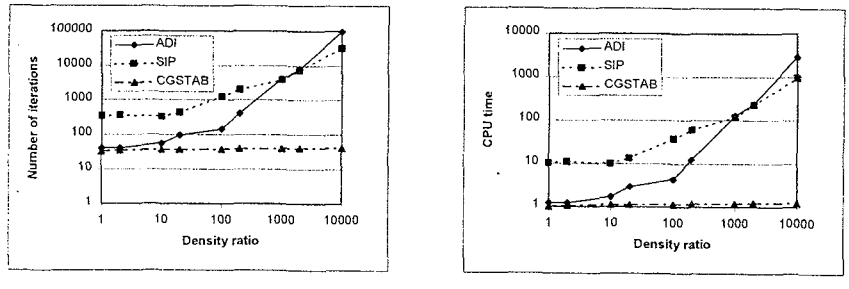

Figure 1: Convergence rate of pressure equation solvers for different density ratios.

3. Results of Basic Test Calculations

The numerical methods used in ESE were precisely tested on a number of carefully chosen problematic basic cases where the analytical solutions are known. These test-cases include phase presence probability shock propagation and velocity shock propagation in cylindrical coordinate system in different directions regarding to the coordinate axes, jet free fall in a vacuum in the absence of any pressure forces, phase generation, compression and expansion under temperature and pressure changes, etc. For each calculation the conservation of mass and momentum was checked and a convergence analysis was performed. The results were compared with the known analytical solutions and the calculations, which were performed using the first order accurate upwind method and the second order accurate Lax-Wendroff method. All test calculations clearly show that the used high-resolution method most exactly reproduces the analytical behavior. In the following we will present some of these results in form of graphs.

3.1 Phase presence probability shock propagation

A phase presence probability shock in the form of a box with phase presence probability $\alpha = 1$ for $(r \in [0.1, 0.3]) \wedge (z \in [0.1, 0.3])$ and $\alpha = 0$ otherwise has been moved with constant velocity $v = 1$ (movement of a big bubble) parallel (Fig.2, Fig.3) and diagonal (Fig.4) to the z and r axis on a mesh 160x160 grid points. The Courant number was 0.5. The convergence analysis, which was performed on meshes 20x20, 40x40, 80x80 and 160x160 grid points, showed that the results obtained with the high-resolution method are approaching to the analytical solution. As expected the upwind method had the highest numerical diffusion and the Lax-Wendroff method produced spurious oscillations and gave unphysical results since the phase presence probability was also negative. The mass has been conserved perfectly by all three numerical methods.

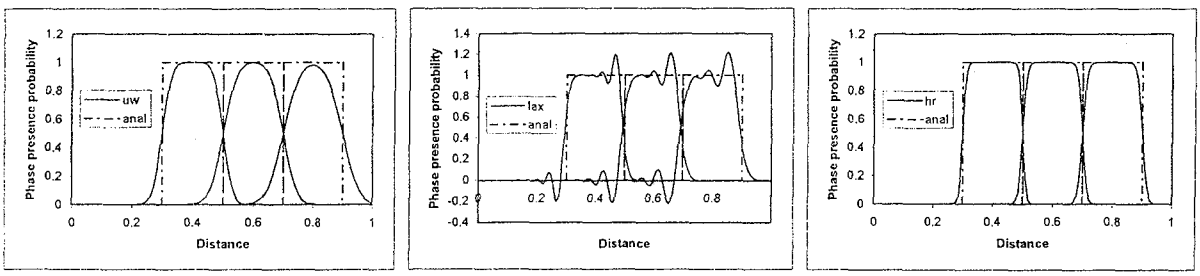

Figure 2: Phase presence probability shock convection in z direction calculated with the upwind, Lax-Wendroff and high-resolution method for different times.

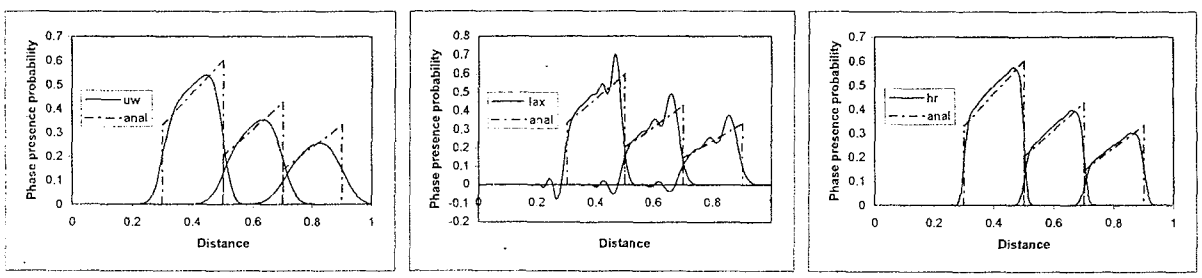

Figure 3: Phase presence probability shock convection in r direction calculated with the upwind, Lax-Wendroff and high-resolution method for different times.

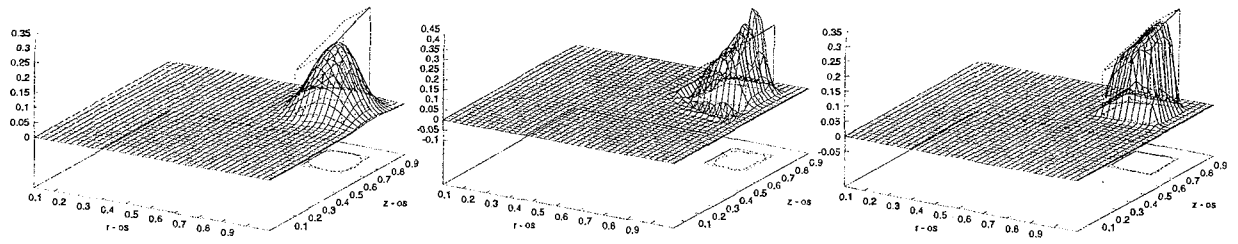

Figure 4: Phase presence probability shock convection diagonal to the r and z axis calculated with the upwind, Lax-Wendroff and high-resolution method.

3.2 Velocity shock propagation

The propagation of a 1D velocity shock in the form of a step has been studied. This situation appears in multiphase flow when for example a molten fuel jet of low phase presence probability moves through resting air. Since the jet velocity is defined only in the jet it is assumed that the jet velocity is equal to the air velocity $v_{jet} = v_{air} \approx 0$ in the region where the jet phase presence probability is zero: $\alpha = 0$. The convergence analysis, which was performed on meshes 20, 40, 80 and 160 grid points, showed that the results obtained do not approach to the analytical solution. The velocity shock did not propagate with the jet speed (Fig.5) despite the improvement (4) and therefore the jet phase presence probability achieved very high unphysical values at the front (Fig.6) also for the high-resolution method. None of the numerical methods conserved the jet momentum either (Fig.7).

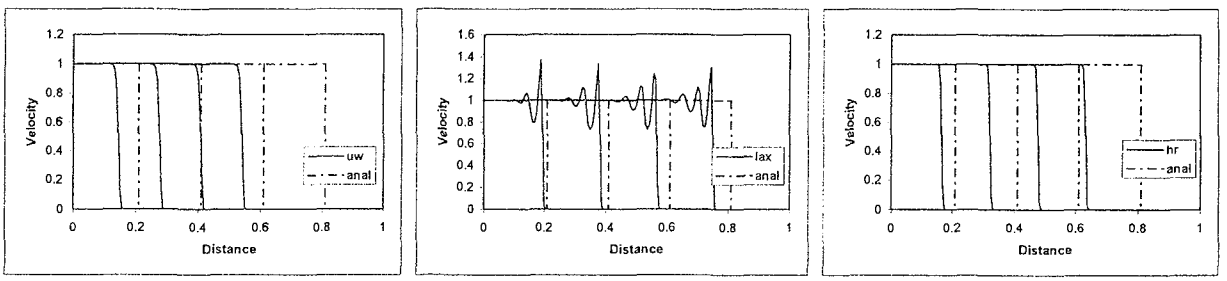

Figure 5: 1D velocity shock propagation calculated with the upwind, Lax-Wendroff and high-resolution method for different times. Courant number = 0.5. Mesh: 160 grid points.

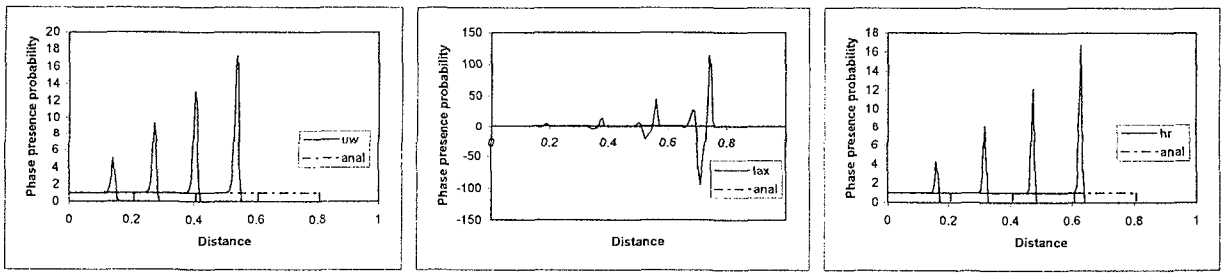

Figure 6: Jet phase presence probability calculated with the upwind, Lax-Wendroff and high-resolution method for different times. Courant number = 0.5. Mesh: 160 grid points.

Since these results are not satisfactory the numerical model was significantly improved with a simple but physically correct prescription that the velocity at the mesh point next to the front where the phase presence probability is zero and therefore the velocity is not defined is equal to the front velocity. With this improvement the convergence analysis showed that the velocity and phase presence probability correctly approach to the analytical solution (Fig.8) and that the mass and momentum are conserved well.

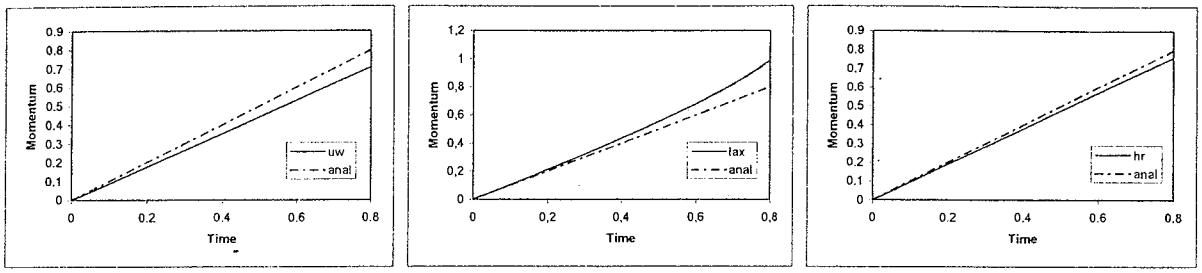

Figure 7: Jet momentum at calculations with the upwind, Lax-Wendroff and high-resolution method. Courant number = 0.5. Mesh: 160 grid points.

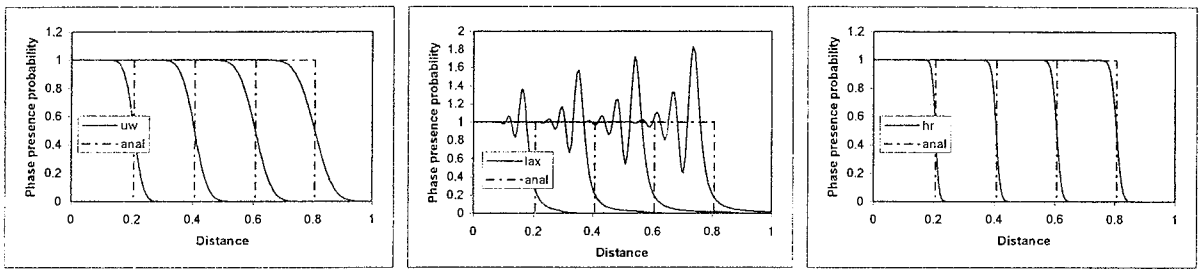

Figure 8: Jet phase presence probability calculated with the improved model for different times. Courant number = 0.5. Mesh: 160 grid points.

3.3 Jet free fall

To check the numerical model on a problem with an ununiform velocity field occurring together with a shock in the jet phase presence probability field and the velocity field, the jet free fall (particles falling in a vacuum in the absence of any pressure forces) has been simulated. The jet phase presence probability and the jet velocity at the inlet boundary were $\alpha = 1$ and $v = 1$. The convergence analysis, which was performed on meshes 20, 40, 80 and 160 grid points, showed that the results obtained using the upwind and high-resolution method approach to the analytical solution (Fig.9), whereas the Lax-Wendroff method produced highly oscillating and divergent results.

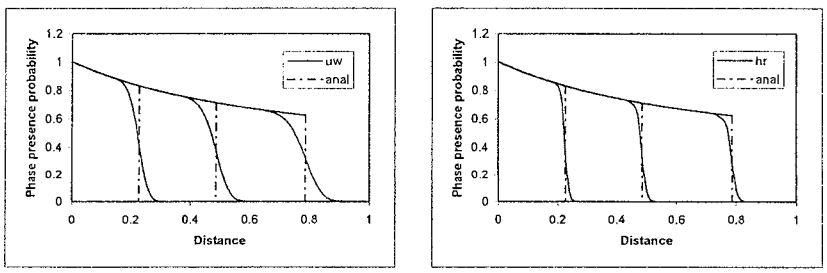

Figure 9: Jet free fall phase presence probability for different times. Courant number = 0.5 Mesh: 160 grid points.

3.4 Phase generation

The correct numerical treatment of the vapor generation term Γ appearing in the mass (1) and pressure (5) equations was established on the following combined artificial test case. An open vessel was filled with two liquids – liquid A occupied the lower part of the vessel and the other liquid B with equal density occupied the upper part. In the middle of the lower part of the vessel liquid A was generated with the generation rate $\Gamma_A = V_{vessel}\rho_A / 1\text{sec}$. The

calculation was performed on mesh sizes 10x15, 20x30, 40x60 and 80x120 grid points in the cylindrical coordinate system. The results of the convergence analysis showed that the upwind and high-resolution methods correctly predicted the phase volume, whereas the Lax-Wendroff method underestimated the phase generation since the phase interface did not move with the right velocity.

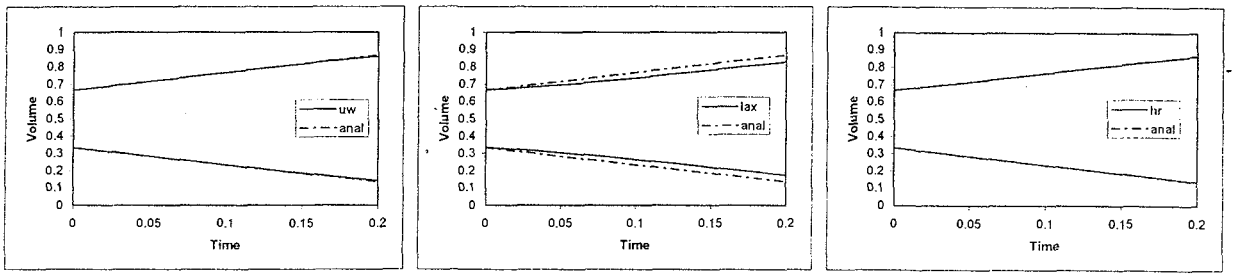

Figure 10: Phase volume of liquid A and B during phase generation of A. Mesh: 10x15 grid points.

3.5 Pressure compression and temperature expansion

The ability of ESE to correctly consider the compressibility $(\partial\rho/\partial p)_h$ and the temperature dependency of density $\rho^{n+1/2} = \rho\left(h^{n+1}, p^n\right)$ was also proved. An open vessel was again filled with two liquids – this time a compressible liquid A with $\chi = 1\,\mathrm{bar}^{-1}$ and temperature dilatation $\beta = 0.005\,\mathrm{K}^{-1}$ occupied the lower part of the vessel and an incompressible liquid B with $\chi = 0\,\mathrm{bar}^{-1}$ and $\beta = 0\,\mathrm{K}^{-1}$ occupied the upper part. The following artificial test cases were simulated:

- the pressure was risen with a speed $dp/dt = 1\,\mathrm{bar/s}$ (Fig.11) at constant temperature,
- the temperature was risen with a speed $dT/dt = 100\,\mathrm{K/s}$ (Fig.12) at constant pressure,
- the vessel was closed and the temperature was risen with a speed $dT/dt = 100\,\mathrm{K/s}$ (Fig.13).

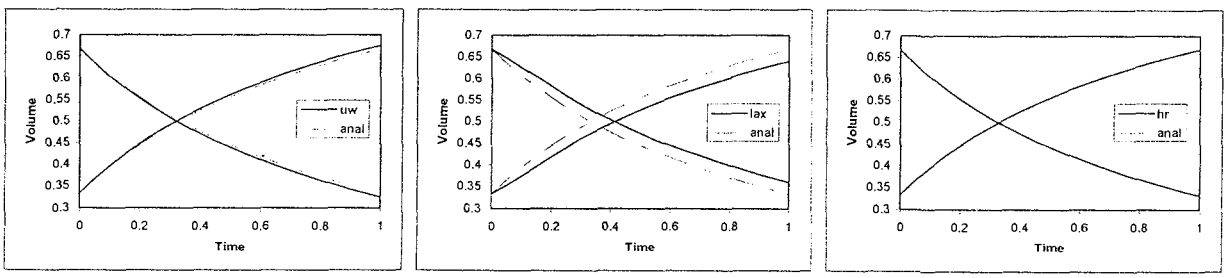

Figure 11: Phase volume of liquid A and B during the pressure rise. Mesh: 10x15 grid points.

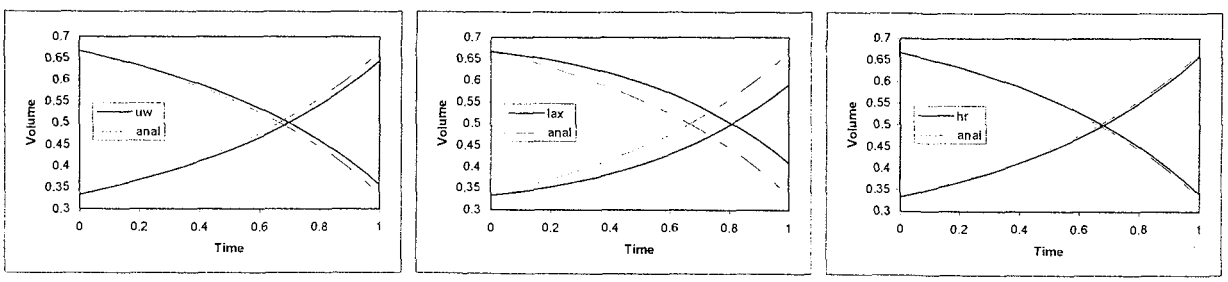

Figure 12: Phase volume of phase A and B during the temperature rise. Mesh: 10x15 grid points.

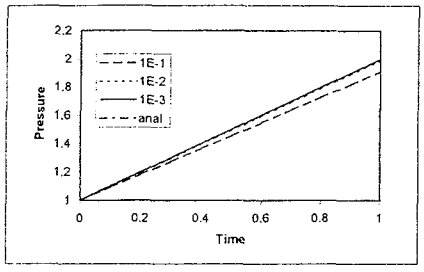

Figure 13: Vessel pressure during the temperature rise. Mesh: 10x15 grid points.

The convergence analysis which was performed on meshes 10x15, 20x30, 40x60 and 80x120 grid points showed that the results of all three methods approach to the analytical solution. The best results, however, were obtained with the high-resolution method.

The results of the third -test case, the temperature rise in the closed vessel, are identical for all three methods, since there is no convection. Here the time step of the calculation was altered (Δt = 1E-1, 1E-2, 1E-3) and it was shown that the pressure rise is correctly predicted if the time step is small enough (Fig.13).

4. Conclusions

The numerical treatment of the probabilistic multiphase flow equations on which ESE is based has been described. ESE (Evaluation of Steam Explosions) is a general two-dimensional compressible multiphase flow code, which has been developed to model the interaction of molten core debris with water during the first premixing stage of a steam explosion.

The mass, momentum and energy equations are solved on a staggered grid in a 2D rectangular or cylindrical coordinate system using a second order accurate high-resolution finite difference method. The pressure equation is solved using the CGSTAB method, which converges fast also for high density ratios.

The numerical methods used in ESE were precisely tested on a number of carefully chosen basic cases where the analytical solutions are known. All test calculations clearly show that the applied high-resolution method most exactly reproduces the analytical behavior.

5. References

[1] J. Marn and M. Leskovar: *Simulation of Steam Explosion Premixing Phase Using Probabilistic Multiphase Flow Equations.* Fluid Mechanics Research. Scripta Technica, Inc., 1996, ISSN 1064-2285/93/0001-0044, 22 (1), pp. 44-55.

[2] D.F. Fletcher and M.K. Denham: *Validation of the CHYMES Mixing Model.* Nuclear Engineering and Design 155, 1995, pp. 85-96.

[3] F.J. Davies, M.F. Young: *Integrated Fuel-Coolant Interaction (IFCI 6.0) Code: User's Manual.* Sandia National Laboratories report SAND94-0406, NUREG/CR/-6211 (1994).

[4] W.H. Amarasooriya, T.G. Theofanous: *Premixing of Steam Explosions: A Three-Fluid Model.* Nucl. Eng.& Design, 126, 23-39, (1991).

[5] G. Berthoud, M. Valette: *Calculations of the Premixing Phase of an FCI with the TRIO MC Code.* Proc. CSNI Specialist Meeting on Fuel Coolant Interactions, Santa Barbara, January 5-8, 1993, NUREG/CP-0127, 27-36 (1993).

[6] H. Jacobs, M. Lummer, L. Meyer, B. Stehle, K. Thurnay, L. Vaeth: *Multifield Simulations of Premixing Experiments.* Proc. CSNI Specialist Meeting on Fuel Coolant Interactions, Santa Barbara, January 5-8, 1993, NUREG/CP-0127, 204-217 (1993).

[7] A. Annunziato, C. Addabbo: *COMETA (Core Melt Thermal-Hydraulic Analysis) a Computer Code for Melt Quenching Analysis.* Proceedings of the International Conference on New Trends in Nuclear System Thermohydraulics, Pisa, June 1994 (1994).

[8] R.J. LeVeque: *Numerical Methods for Conservation Laws.* Lectures in Mathematics ETH Zurich, Birkhauser Verlag, Basel, 1992, ISBN 3-7643-2723-5.

[9] J. Marn and M. Leskovar: *Probabilistic Multiphase Flow Equations: Simulation of Three Phase Mixture.* ASME FED Summer Meeting, Proceedings (1996), FED-Vol.236, Vol.1, pp. 161-165.

[10] J.H. Ferziger, M. Perič: *Computational Methods for Fluid Dynamics.* Springer-Verlag, Berlin, Heidelberg, 1996.